Journal of Materials Chemistry C

PAPER

View Article Online
View Journal | View Issue

Cite this: J. Mater. Chem. C, 2019, 7, 14563

Functionalizing tetraphenylpyrazine with perylene diimides (PDIs) as high-performance nonfullerene acceptors†

Gang Li,‡*[a] Shufan Yang,‡[a] Tao Liu,*[ab] Jiewei Li,[c] Wenbin Yang,[a] Zhenghui Luo,[b] Cenqi Yan,[a] Dandan Li,[a] Xinyu Wang,[a] Guanwei Cui,[a] Tao Yang,[d] Liang Xu,[e] Shun-Ze Zhan,[e] Lijun Huo,*[f] He Yan*[b] and Bo Tang*[a]

Received 15th October 2019,
Accepted 25th October 2019

DOI: 10.1039/c9tc05643b

rsc.li/materials-c

Perylene diimide (PDI)-based small molecular acceptors with a three-dimensional structure are thought to be essential for efficient photocurrent generation and high power conversion efficiencies (PCEs). Herein, a couple of new perylene diimide acceptors (PPDI-O and PPDI-Se) have been designed and successfully synthesized using pyrazine as the core-flanking pyran and selenophene-fused PDIs, respectively. Compared to PPDI-O, PPDI-Se exhibits a blue-shifted absorption in the 400–600 nm range, a comparable LUMO level, and a more distorted molecular geometry. The PPDI-Se-based organic solar cell device with PDBT-T1 as the donor achieved the highest PCE of 7.47% and a high open-circuit voltage (V_{oc}) of up to 1.05 V. The high photovoltaic performance of PPDI-Se-based devices can be attributed to its high LUMO energy level, complementary absorption spectra with donor materials, favorable morphology and balanced carrier transport. The results demonstrate the potential of this type of fullerene-free acceptor for high efficiency organic solar cells.

Introduction

In the past three decades, organic solar cells (OSCs), composed of bulk heterojunction (BHJ) structure with p-type polymer donor and n-type small molecular acceptor, have been proven to be promising candidates for next-generation photovoltaic technology and have aroused great interest among the scientific community.[1–5] With regard to conventional acceptor molecules, fullerene derivatives, such as [6,6]-phenyl-C61-butyric acid methyl ester ($PC_{61}BM$) and [6,6]-phenyl-C71-butyric acid methyl ester ($PC_{71}BM$) have benefited from their high electron affinity, isotropic electron transport, and large electron mobility.[6–11] Therefore, fullerene-based OSCs have moved into the fast lane, and the power conversion efficiency (PCE) of single-junction OSCs have exceeded 10%.[12–14] However, the inherent defects of the fullerene derivatives restrict the further improvement of device performances assigned to limited optical cross-section as well as poor environmental and phase stability issues.[15–18] Therefore, non-fullerene small molecule acceptors (SMAs) emerged as great strides to OSC development.[19,20] Except for the merits of low-cost, light weight, and mechanism flexibility, SMAs also show substantially strong absorption in the visible region, relatively simple synthesis and purification, easy modulation of their energy levels through developing versatile molecular structures, and morphological compatibility with different types of donor materials.[21,22] So far, a number of SMAs have been developed and applied in OSCs that have achieved PCEs exceeding 13%,[23–36] which outperformed those of $PC_{61}BM$/$PC_{71}BM$-based counterparts. To date, highly efficient OSCs almost exclusively are focused on indacenodithiophene (IDT) or indacenodithienothiophene (IDTT) donor building blocks and 1,1-dicyanomethylene-3-indanone (IC) acceptor moiety.[37–40] However, the superiority of the non-fullerene acceptors consisting of other structures is quite rare. Thus, continued progress will require the design, synthesis, and testing of new motifs for electron acceptors.[41]

[a] College of Chemistry, Chemical Engineering and Materials Science, Key Laboratory of Molecular and Nano Probes, Ministry of Education, Collaborative Innovation Center of Functionalized Probes for Chemical Imaging in Universities of Shandong, Institute of Materials and Clean Energy, Shandong Provincial Key Laboratory of Clean Production of Fine Chemicals, Shandong Normal University, Jinan 250014, P. R. China. E-mail: ligang@sdnu.edu.cn, tangb@sdnu.edu.cn
[b] Department of Chemistry and Energy Institute, The Hong Kong University of Science and Technology, Clear Water Bay, Hong Kong. E-mail: Liutaozhx@ust.hk;hyan@ust.hk
[c] Key Laboratory of Flexible Electronics (KLOFE) & Institute of Advanced Materials (IAM), Jiangsu National Synergetic Innovation Center for Advanced Materials (SICAM), Nanjing Tech University (NanjingTech), 30 South Puzhu Road, Nanjing, 211816, P. R. China
[d] Key Laboratory of Biofuels, Qingdao Institute of Bioenergy and Bioprocess Technology, Chinese Academy of Sciences, P. R. China
[e] Key Laboratory for Preparation and Application of Ordered Structural Materials of Guangdong Province, Shantou University, Shantou 515063, P. R. China
[f] School of Chemistry, Beihang University, Beijing 100191, P. R. China. E-mail: huolijun@buaa.edu.cn

† Electronic supplementary information (ESI) available: Details of synthesis and characterization. See DOI: 10.1039/c9tc05643b

‡ These authors contributed equally to the work.

Perylene diimide (PDI) derivatives, which are classic industrial dyes, have been widely used to construct high-performance SMAs owing to high electron affinity and mobility, intense absorption, and excellent thermal and photochemical stability.[42–45] Furthermore, PDIs can be functionalized in various positions, for example imide, bay and ortho positions, to construct versatile PDI derivatives.[46–49] Hence, incremental endeavors have been devoted to developing high-performance PDI-based SMAs. However, their flat configurations and π-conjugated polyaromatic core are inclined to form microscale or submicroscale aggregates, which hamper the exciton diffusion, charge transport, and collection to the electrodes.[50] Hence, the twisted three-dimensional (3D) structures were adopted to suppress aggregation trends. However, the twisted structures induced by steric congestion among the PDI units will reduce their charge transport abilities and impede the further improvement in the OSC performance.[51,52] Hence, chalcogen-fused PDIs have been actively investigated recently for overcoming the problems mentioned above. For example, Wang *et al.* developed S/Se annulated PDI dimers (s-diPBI-S and s-diPBI-Se) as splendid acceptors. Both acceptors exhibited quite twisted configurations due to the large steric repulsion, and high PCEs of 7.16% and 8.4% were achieved by using PDBT-T as a donor.[53,54] Yan *et al.* used the ring-fusion strategy to obtain a PDI tetramer named FTTB-PDI4 with a "double-decker" molecular shape, which demonstrated an outstanding PCE of 10.58% when combined with the polymer P3TEA.[55] Accordingly, these promising properties with 3D architecture and chalcogen-decorated PDIs have proved to be effective in designing highly efficient SMAs. Despite the great progress that has been achieved in the conjugated multidimensional PDIs, it has not yet reached the stage of commercialization. Thus, the development of PDIs based high-efficiency OSCs and further understanding of their optoelectronic properties and structure–property relationships remains the key issue that the scientists from the fields of chemistry and material science need to focus on.

In this study, to take advantage of the chalcogen-decorated PDIs and investigate the impact of different chalcogen-fused PDIs acceptors on the photovoltaic properties, a couple of low-cost SMAs (PPDI-O and PPDI-Se), which employed tetraphenylpyrazine as the central 3D conformation core and were armed by four pyran and selenophene fused PDI motifs, were designed and successfully synthesized (Scheme 1). The influence of the molecular geometry on the OSC performance was investigated by studying the optical, photophysical, and morphological properties in the BHJ blended films. As a result, the OSCs based on PPDI-Se delivered a maximum PCE of 7.47% with an open-circuit voltage (V_{oc}) of 1.05 V, a short-circuit current (J_{sc}) of 10.7 mA cm^{-2}, and a fill factor (FF) of 66.3%, which were superior to those of the PPDI-O based device (PCE = 4.51%). These remarkable results demonstrated that PPDI-Se is an excellent acceptor for achieving favorable efficiency.

Results and discussion

Material synthesis and characterization

The syntheses of PPDI-O and PPDI-Se are displayed in Scheme 1. First, compound PDI-NO_2 was converted to PDI-Se in *N*-methylpyrrolidone with selenium powder at 190 °C. Subsequently, PDI-Se-Br was synthesized by brominating the compound PDI-Se under dichloromethane at room temperature.[54] Then, PPDI-Se was obtained by the Suzuki-coupling of borylated tetraphenylpyrazine and PDI-Se-Br. The synthetic method of PPDI-O was similar to that of PPDI-Se, according to our reported method.[56] The as-synthesized new molecules were fully characterized by ^{1}H NMR, ^{13}C NMR, and

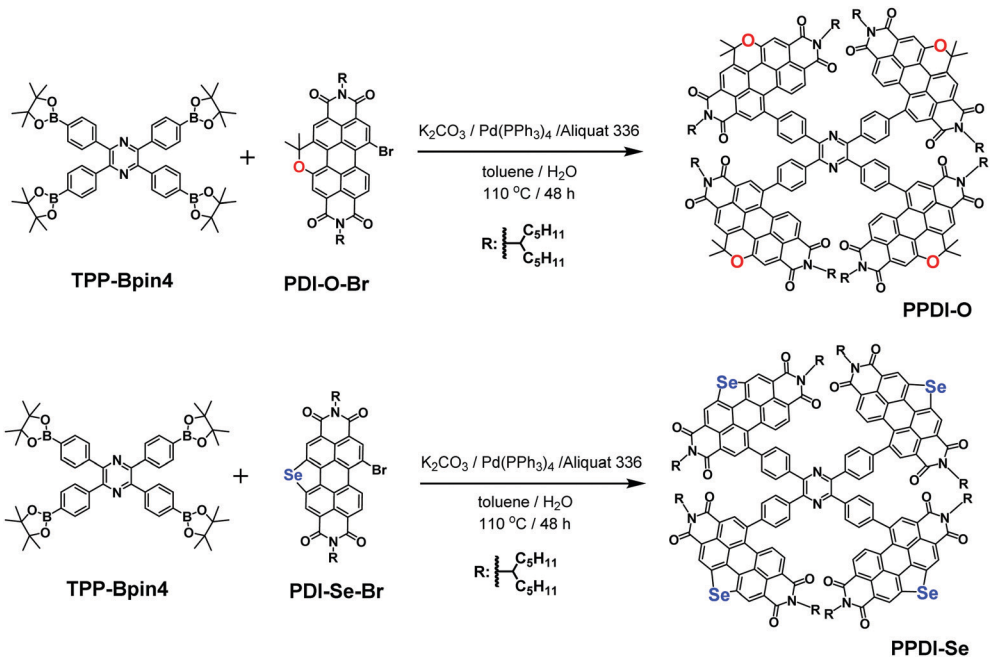

Scheme 1 The synthesis routes of PPDI-O and PPDI-Se.

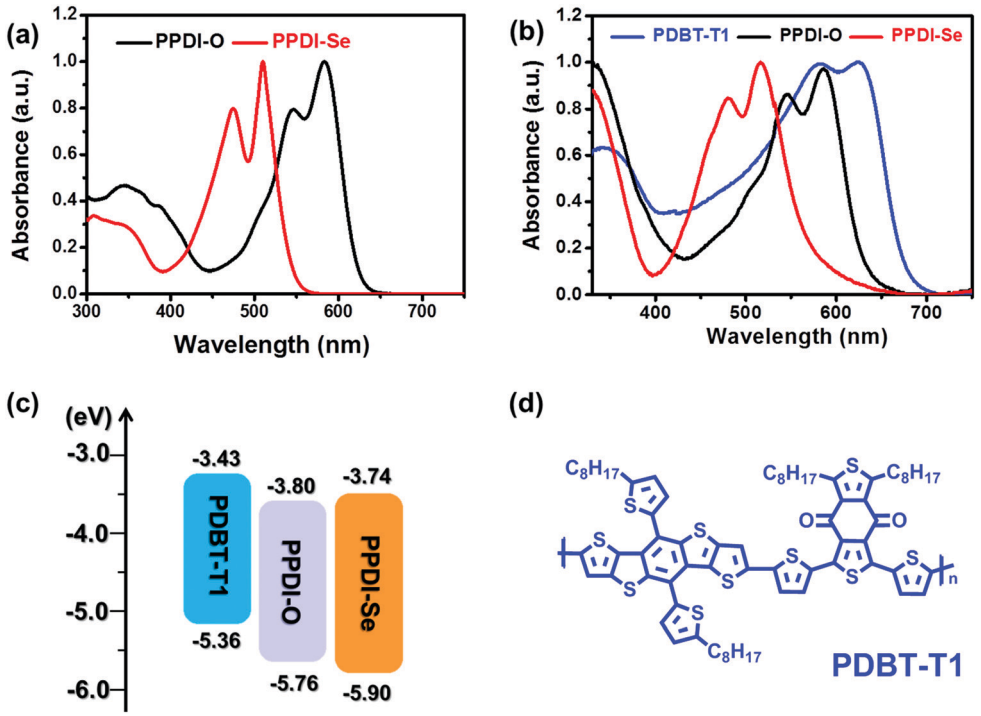

Fig. 1 (a) Absorption spectra of PPDI-O and PPDI-Se in chloroform solutions. (b) Absorption spectra of PBDB-T1, PPDI-O and PPDI-Se in thin films state. (c) Energy level diagrams of the involved materials in organic solar cells. (d) The molecular structure of donor PDBT-T1.

MALDI-TOF mass spectrometry. Furthermore, the two molecules, *i.e.*, PPDI-O and PPDI-Se were found to be highly soluble in most of the commonly used organic solvents, for example, dichloromethane, chloroform, chlorobenzene, and *o*-dichlorobenzene. Thermogravimetric analysis measurements (Fig. S15, ESI†) demonstrated that both compounds exhibited good thermal stability, with a decomposition temperature (T_d, 5% weight loss) exceeding 300 °C under nitrogen atmosphere.

Optical and electrochemical properties

The normalized UV-vis absorption spectra of PPDI-O and PPDI-Se in chloroform solutions and in the form of thin films were measured and presented in Fig. 1a and b, with the spectral data being summarized in Table 1. The solution spectrum of PPDI-O exhibited strong absorption from 450–650 nm, with an absorption maximum (λ_{max}) at 583 nm, while the λ_{max} of PPDI-Se blue-shifted by 73 nm compared with that of its PPDI-O counterpart. In the thin-film state, both PPDI-O and PPDI-Se spectra exhibited red shift and broader absorption than their corresponding solution spectra, with the maximum absorption peak at 586 nm for PPDI-O and 515 nm for PPDI-Se. The blue-shifted absorption of PPDI-Se relative to PPDI-O, can form more obvious complementary absorption with donor of PDBT-T1 (Fig. 1d), which are beneficial in enhancing light harvesting, so as to increase J_{sc}. The optical edges of the thin film are 1.96 and 2.16 eV for PPDI-O and PPDI-Se, respectively, which were consistent with the theoretically calculated results (Table S1, ESI†).

Cyclic voltammetry (CV) was performed to investigate the electrochemical properties of PPDI-O and PPDI-Se (Fig. S1, ESI†), and the data are summarized in Table 1. The lowest unoccupied molecular orbital (LUMO) energy levels of PPDI-O and PPDI-Se were estimated to be −3.80 and −3.74 eV, respectively, according to the equation $E_{LUMO} = -e(E_{red} + 4.80)$ (eV),[55] assuming that Fc/Fc^+ was −4.80 eV. The energy level of HOMO can be calculated from the following equation: $E_{HOMO} = -(E_{LUMO} + E_g)$ eV, and found to be −5.76 and −5.90 eV for PPDI-O and PPDI-Se, respectively. As expected, both acceptors exhibited relatively upshifted LUMO energy levels, which were beneficial for obtaining higher V_{oc} in the corresponding OSC devices.

Theoretical analysis

The geometries of PPDI-O and PPDI-Se were obtained by employing the density functional theory (DFT) method at the

Table 1 Basic Properties of PPDI-O and PPDI-Se

Acceptors	$\lambda_{max}{}^a$ (nm)	$\varepsilon_{max}{}^a$ (M^{-1} cm^{-1})	$\lambda_{onset}{}^a$ (nm)	$\lambda_{max}{}^b$ (nm)	$\lambda_{onset}{}^b$ (nm)	$E_g^{opt\ c}$ (eV)	HOMO (eV)	LUMO^d (eV)
PPDI-O	583	1.36×10^5	620	586	630	1.96	−5.76	−3.80
PPDI-Se	510	1.72×10^5	545	516	572	2.16	−5.90	−3.74

[a] In a dichloromethane solution. [b] In a neat film. [c] Calculated from empirical the formula: $E_g^{opt} = 1240/\lambda_{onset}$. [d] Cyclic voltammetry(CV) method by measuring in dichloromethane.

Table 2 Performance of the optimized OSCs devices based on PDBT-T1:PPDI-O and PDBT-T1:PPDI-Se (1 : 1, w/w)

Active layer	Additive	V_{oc}[a] (V)	J_{sc}[a] (mA cm^{-2})	J_{sc}[b] (mA cm^{-2})	FF (%)	PCE[a] (%)
PDBT-T1:PPDI-O	0.25% DIO	1.03 (1.03 ± 0.004)	8.51 (8.45 ± 0.197)	8.14	51.1 (49 ± 0.015)	4.51 (4.29 ± 0.180)
PDBT-T1:PPDI-Se	0.25% DIO	1.05 (1.05 ± 0.006)	10.7 (10.5 ± 0.202)	10.5	66.3 (65 ± 0.016)	7.47 (7.21 ± 0.217)

[a] Values are for the highest-PCE device, with the average values obtained from 20 devices listed in parentheses. [b] J_{sc} value from the integration of the EQE spectra.

B3LYP/6-31G(d,p) level in the Gaussian 09 software,[57] where the long alkyl chain (–$C_{11}H_{23}$) was simplified to isopropyl groups. The original configurations (input-configurations in Gaussian) of PPDI-O and PPDI-Se were similar. Based on the optimized geometries, the frontier molecular orbitals and the corresponding energy levels were calculated (Fig. S2, ESI†). The HOMO and LUMO of PPDI-O are delocalized on two pyran-fused PDI subgroups, respectively. On the other hand, the HOMO and LUMO of PPDI-Se are localized on one selenophene fused PDI sub-group. The different wave function distribution between PPDI-O and PPDI-Se are mainly due to the degenerate orbitals of the same four groups. In addition, the dihedral angle between the PDI unit and the adjacent benzene ring for PPDI-O (Fig. S3, ESI†) was calculated to be 61.39°, 61.41°, 62.61°, and 62.65°. On the other hand, in the case of PPDI-Se, the corresponding dihedral angle (Fig. S4, ESI†) was found to be 63.51°, 72.72°, 73.99°, and 74.50°. The more twisted geometry of PPDI-Se was expected to effectively prevent the four PDI units from forming the large aggregate domains in the solid-state, which is beneficial for the PDI blend film applied in the OSCs.[5] The calculated HOMOs and LUMOs of PPDI-O and PPDI-Se were found to be −5.87 and −3.55 eV and −6.13 and −3.59 eV (Table S1, ESI†), respectively, which are in accordance with the changing trend of the energy levels measured by the CV method.

Photovoltaic properties

The OPV devices of these two new electron acceptors were fabricated and evaluated with a conventional device structure of ITO (indium tin oxide)/PEDOT:PSS(poly(3,4-ethylenedioxythiophene):poly (styrene sulfonate))/PDBT-T1:acceptor/ZrAcAc (zirconium acetylacetonate)/Al. The detailed device fabrication processes are described in the supporting information. A medium-bandgap polymer PDBT-T1 was chosen as the polymer donor due to its complementary absorption and matched energy levels with PPDI-O and PPDI-Se (Fig. 1c). We selected DCB as a processing solvent and 100 °C as the annealing temperature. The total concentration of donor and acceptor was selected to be 20 mg mL^{-1}, with the donor : acceptor weight ratio of 1 : 1. The optimized device parameters are summarized in Table 2, with the corresponding *J–V* curves shown in Fig. 2a. The optimized OSC device based on PDBT-T1:PPDI-Se exhibited a high PCE of 7.48% with a high V_{oc} of 1.05 V, J_{sc} of 10.7 mA cm^{-2}, and FF of 66.3%, while PDBT-T1:PPDI-O based devices achieved an inferior PCE of 4.51%, with similar V_{oc} of 1.04 V, lower J_{sc} of 8.51 mA cm^{-2}, and relatively poor FF of 51.1%. Compared with PPDI-O, the substantial superiority of PPDI-Se-based OSC performances can be attributed to the preferable J_{sc} and FF.

The external quantum efficiency (EQE) spectra of the blend films were acquired from two different NFA-based devices and displayed in Fig. 2b. The variation in the calculated J_{sc} by the integration of the EQE spectra was found to be consistent with the variation in the measured J_{sc} (Table 2). Significant enhancement of EQE responses between 350 and 700 nm for the PDBT-T1:PPDI-Se-based device can be attributed to the much more complementary absorption from PPDI-Se and PDBT-T1. Overall, the greater optical absorption range of the PPDI-Se blend relative to PPDI-O blends was unequivocally confirmed from the greater J_{sc} value (10.7 *versus* 8.51 mA cm^{-2}).

Morphology characterization

The morphology of the BHJ films is known to be closely correlated to J_{sc}, mobility, and PCE. Thus, the atomic force microscopy (AFM) amplitude and phase images in the tapping mode were obtained to characterize the morphology of PDBT-T1:PPDI-O and PDBT-T1:PPDI-Se active layers (Fig. S5, ESI†). The optimized PDBT-T1:PPDI-O blend film showed a smooth surface, with a relatively small root-mean-square (RMS) roughness of 1.01 nm, but clear phase separation was not observed (Fig. S4a and c, ESI†). In contrast,

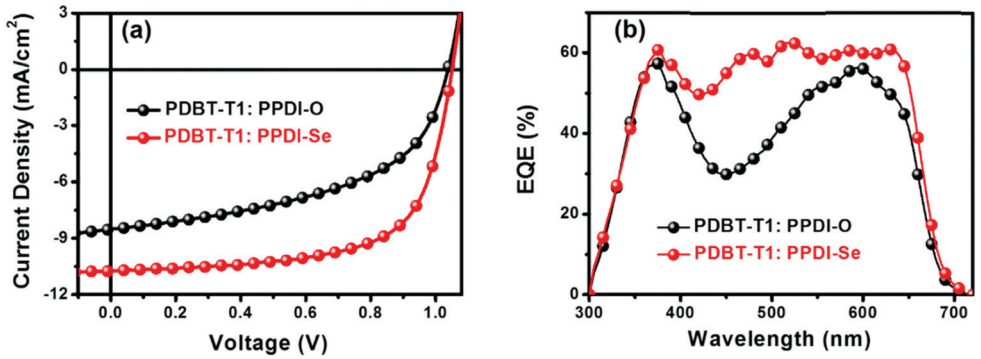

Fig. 2 (a) Characteristic *J–V* curves of the PDBT-T1:PPDI-O and PDBT-T1:PPDI-Se based solar cells under AM 1.5G irradiation (100 mW cm^{-2}). (b) EQE curves of the corresponding devices.

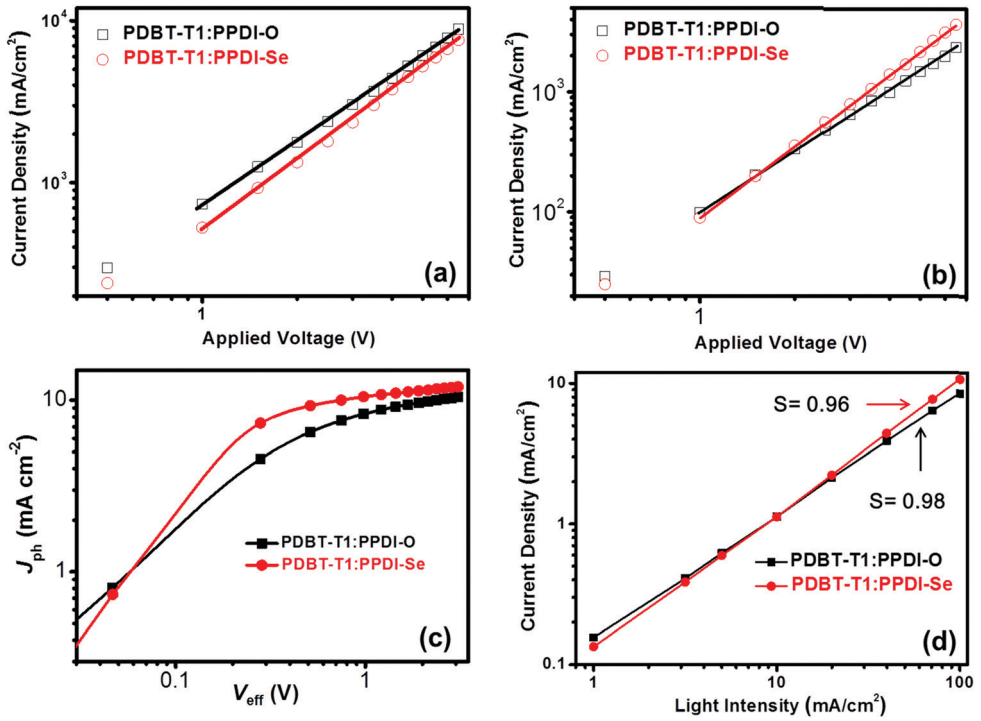

Fig. 3 Dark current density–voltage characteristics for (a) hole-only and (b) electron-only devices with optimized PDBT-T1:PPDI-O and PDBT-T1:PPDI-Se BHJ films. (c) J_{ph} *versus* V_{eff} curves. (d) Light intensity dependence of J_{sc}.

the PDBT-T1:PPDI-Se-based blend film showed a slightly higher RMS of 1.07 nm and better defined fibril texture (Fig. S4b and d, ESI†) with suitable phase separation, which are beneficial for exciton dissociation and charge transport, and thus lead to better photovoltaic performance. The morphologies of the PDBT-T1:PPDI-O and PDBT-T1:PPDI-Se blend films were also characterized by transmission electron microscopy (TEM) to better understand the BHJ morphologies in the devices. As shown in Fig. S6 (ESI†), the TEM images showed similar nanofibrillar structures of both the blend systems.

Active layer charge transport

To investigate the charge-transporting behavior and explore the reasons for the different FF of the studied devices, the hole (μ_h) and electron mobilities (μ_e) of the blend films were evaluated through the space charge limited current (SCLC) method (Fig. 3a and b). The electron mobilities of both the acceptor neat films were found to be 5.32×10^{-4} and 6.57×10^{-4} cm^2 V^{-1} s^{-1}, respectively. When blended with the donor of PDBT-T1, the PDBT-T1:PPDI-Se-based blend film exhibited relatively higher and more balanced hole and electron mobilities ($\mu_h = 6.51 \times 10^{-4}$ cm^2 V^{-1} s^{-1}, $\mu_e = 3.40 \times 10^{-4}$ cm^2 V^{-1} s^{-1}, and $\mu_h/\mu_e = 1.91$) compared with the PDBT-T1:PPDI-O counterpart ($\mu_h = 6.24 \times 10^{-4}$ cm^2 V^{-1} s^{-1}, $\mu_e = 2.78 \times 10^{-4}$ cm^2 V^{-1} s^{-1}, and $\mu_h/\mu_e = 2.24$), which results in efficient charge transport and corresponds to higher FF for the PDBT-T1:PPDI-Se-based device.[58]

Exciton dissociation and charge extraction

In order to further study the exciton dissociation, charge recombination and charge extraction properties of the above-mentioned devices, the photocurrent density (J_{ph}) *versus* the effective applied voltage (V_{eff}) curves were determined (Fig. 3c), where $J_{ph} = J_L - J_D$ (J_L and J_D are the current density under illumination and dark, respectively) and $V_{eff} = V_0 - V_a$, (V_0 is the voltage at $J_{ph} = 0$ and V_a is the measured voltage under different current density). PDBT-T1:PPDI-Se demonstrated a higher J_{ph} of 10.734 mA cm^{-2} than the PDBT-T1:PPDI-O-based device, which exhibited J_{ph} of 8.51 mA cm^{-2} at $V_{eff} \geq 2.0$ V. This was mainly caused by the much higher light absorbing combination of PDBT-T1:PPDI-Se. The charge dissociation and collection probability (P) could be assessed by the formula $P = J_{ph}/J_{sat}$. Under the short-circuit condition, the probabilities of exciton dissociation for the PDBT-T1:PPDI-O-bases and PDBT-T1:PPDI-Se-based devices were estimated to be 81.7% and 89.5%, respectively. Moreover, the probabilities of charge collection at the maximal power output condition were determined to be 50.7% and 74.2% for PDBT-T1:PPDI-O-based and PDBT-T1:PPDI-Se-based OSCs, respectively. Hence, we can infer that PDBT-T1:PPDI-Se showed superior charge dissociation and collection probability, which is beneficial to the resulting J_{sc} and FF.

Charge-recombination mechanism

The carrier recombination kinetics of PPDI-O-based and PPDI-Se-based devices were also investigated through J–V curves under different light intensities (P_{light}), with the curves being shown in Fig. 3d. The power-law exponents (α) for the two acceptor-based devices were extracted according to the formula $J_{sc} \propto P_{light}^{S}$, where S approaching 1 implies that the bimolecular recombination is negligible. The S values of the two devices were found to be 0.96 (PDBT-T1:PPDI-O) and 0.98 (PDBT-T1:PPDI-Se),

thus suggesting the less bimolecular recombination in the PPDI-Se based devices.

Fig. S7 (ESI†) reveals the dependence of V_{oc} on various light intensities (P_{light}), giving the relationship $V_{oc} \propto (nkT/q)\ln(P_{light})$, where $n = 1$ suggests only bimolecular charge recombination, but $n > 1$ suggests defect-mediated recombination. The n values for PDBT-T1:PPDI-O and PDBT-T1:PPDI-Se were fitted to be 1.26 and 1.74, respectively. This indicates that the bimolecular recombination dominates in the device based on the PDBT-T1:PPDI-O-based device, whereas the defect-mediated charge recombination dominates in the PDBT-T1:PPDI-Se-based device.

Conclusions

In summary, two new small molecule acceptors, PPDI-O and PPDI-S, consisting of a tetraphenylpyrazine core and peripheral chalcogen-decorated perylene diimides, were successfully synthesized and characterized. Compared with the pyran-fused PDI (PPDI-O), the incorporation of the Se atom (PPDI-Se) exhibited an obviously blue-shifted optical absorption, improved and more balanced charge transport properties, and more favorable blend film morphology. BHJ OSCs based on PPDI-Se and PDBT-T1 achieved a high PCE of 7.47% with improved V_{oc} of 1.05 V, a well-maintained J_{sc} of 10.7 mA cm^{-2} despite its blue-shifted absorption, and FF of 66.3%. This result successfully demonstrates that building 3D structures with an extended effective π-conjugation could be a promising methodology to aspire highly efficient PDI-based acceptors.

Experimental section

Synthesis of PPDI-O

A Schlenk tube was initially charged with TPP-Bpin4 (216 mg, 0.243 mmol, 1 eq.), compound PDI-O-Br (1.12 g, 1.338 mmol, 5.5 eq.), $Pd(PPh_3)_4$ (100 mg, 0.017 mmol), anhydrous K_2CO_3 (9.68 g, 70 mmol), Aliquat 336 (4 drops), and dry toluene/H_2O (70 mL/35 mL), and then, the mixture was degassed with nitrogen for 15 min. Subsequently, the reaction mixture was heated at 120 °C for 48 h. After cooling to room temperature, the reaction mixture was extracted by CH_2Cl_2. The crude product was purified by silicon chromatography (petroleum ether/CH_2Cl_2) to get the pure product as a red solid (536 mg, yield 65%). ^{1}H NMR (400 MHz, $CDCl_3$): δ 8.55 (d, 1H), 8.42 (d, 1H), 8.15–7.96 (m, 5H), 7.64 (d, 2H), 5.17–5.05 (m, 2H), 2.22–1.94 (m, 10H), 1.94–1.73 (m, 4H), 1.43–1.18 (m, 24H), 0.88–0.76 (m, 12H). ^{13}C NMR (100 MHz, $CDCl_3$): δ 164.95, 164.45, 163.84, 163.52, 152.18, 147.43, 143.58, 140.73, 138.50, 136.51, 134.54, 133.29, 133.07, 132.00, 130.19, 128.64, 127.88, 126.99, 126.81, 126.30, 124.43, 122.43, 121.87, 116.33, 80.75, 54.79, 54.60, 32.35, 32.20, 31.74, 31.66, 29.71, 29.03, 26.60, 26.50, 22.70, 22.53, 22.48, 14.12, 14.03, 13.98. HRMS: $C_{224}H_{244}N_{10}O_{20}$ (M^+): calcd – 3395.8; found – 3395.8.

Synthesis of PPDI-Se

A Schlenk tube was initially charged with TPP-Bpin4 (216 mg, 0.243 mmol, 1 eq.), compound PDI-Se-Br (1.14 g, 1.338 mmol, 5.5 eq.), $Pd(PPh_3)_4$ (100 mg, 0.017 mmol), anhydrous K_2CO_3 (9.68 g, 70 mmol), Aliquat 336 (4 drops), and dry toluene/H_2O (70 mL/35 mL) and then, the mixture was degassed with nitrogen for 15 min. Subsequently, the reaction mixture was heated at 120 °C for 48 h. After cooling to room temperature, the reaction mixture was extracted by CH_2Cl_2. The crude product was purified by silicon chromatography (petroleum ether/CH_2Cl_2) to get the pure product as a red solid (380 mg, yield 45%). ^{1}H NMR (400 MHz, $CDCl_3$): δ 9.39 (d, 2H), 8.85 (s, 1H), 8.50 (s, 1H), 8.34 (d, 3H), 7.81 (d, 2H), 5.36–5.06 (m, 2H) 2.26–2.02 (m, 4H), 1.86–1.71 (m, 4H), 1.26–1.16 (m, 24H), 0.80–0.72 (m, 12H). ^{13}C NMR (100 MHz, $CDCl_3$): δ 165.24, 164.89, 164.07, 163.83, 147.66, 143.20, 141.37, 140.72, 140.05, 138.83, 134.78, 134.62, 134.05, 132.01, 131.20, 129.39, 128.87, 128.56, 126.52, 126.19, 126.06, 125.83,122.51, 54.99, 54.73, 33.71, 32.38, 32.22, 31.94, 31.74, 31.65, 30.17, 29.71, 29.37, 26.63, 26.52, 23.19, 22.70, 22.53, 22.48, 14.12, 14.01, 13.96. HRMS: $C_{212}H_{119}N_{10}O_{16}Se_4$ (M^+ – H): calcd – 3480.3445; found – 3480.3443.

Fabrication and characterization of photovoltaic cells

Solar cells were fabricated in a conventional device configuration of ITO/PEDOT: PSS/active layer/ZrAcAc/Al. The ITO substrates were first scrubbed by detergent and then sonicated with deionized water, acetone, and isopropanol, in sequence, and dried overnight in an oven. The glass substrates were then treated by UV–Ozone for 30 min before use. A PEDOT:PSS (Heraeus Clevios P VP A 4083) layer was spin-cast onto the ITO substrates at 4000 rpm for 40 s, and then dried at 150 °C for 15 min in air. The donor : acceptor blends with 1 : 1 ratio were dissolved in dichlorobenzene (the concentration of blend solutions was 20 mg mL^{-1} for all blend films) and stirred overnight in a nitrogen-filled glove box. The blend solution was then spin-cast at 1600 rpm for 40 s on the top of PEDOT:PSS layer, followed by annealing at 100 °C for 5 min to remove the residual solvent. A thin ZrAcAc layer (10 nm) and Al layer (100 nm) were sequentially evaporated through a shadow mask under the vacuum of 5×10^{-5} Pa. The area of each device was 5.90 mm^2, as defined by a shadow mask. The optimal blend thickness was about 95 nm, measured on a Bruker Dektak XT stylus profilometer. Current density–voltage (J–V) curves were measured in a Keithley 2400 Source Measure Unit. Photocurrent was measured in an Air Mass 1.5 Global (AM 1.5 G) solar simulator (Class AAA solar simulator, Model 94063A, Oriel) with an irradiation intensity of 100 mW cm^{-2}, which was measured by a standard Si diode (with KG5 filter, purchased from PV Measurement to bring the spectral mismatch to unity). EQEs were measured using an Enlitech QE-S EQE system equipped with a standard Si diode. Monochromatic light was generated from a Newport 300 W lamp source.

Conflicts of interest

There are no conflicts to declare.

Acknowledgements

This study was financially supported by the National Natural Science Foundation of China (No. 21535004, 21927811, 91753111), the Key Research Development Program of Shandong Province

(2018YFJH0502) and Shandong Province Natural Science Foundation (ZR2016BM24). This work is also supported by the Science and Technology Commission of the Military Commission of China, with the project No. 18-H863-00-TS-002-006-01. These authors gratefully acknowledge Prof. Lian-Ming Yang and Fengting Li from Institute of Chemistry, Chinese Academy of Sciences for the MALDI-TOF characterization.

Notes and references

1 Y. Li, *Acc. Chem. Res.*, 2012, **45**, 723.
2 G. Li, R. Zhu and Y. Yang, *Nat. Photonics*, 2012, **6**, 153.
3 Q. F. Xue, R. X. Xia, C. J. Brabec and H. L. Yip, *Energy Environ. Sci.*, 2018, **11**, 1688.
4 S. X. Dai and X. W. Zhan, *Adv. Energy Mater.*, 2018, **8**, 1800002.
5 G. Y. Zhang, J. B. Zhao, P. C. Y. Chow, K. Jiang, J. Q. Zhang, Z. L. Zhu, J. Zhang, F. Huang and H. Yan, *Chem. Rev.*, 2018, **118**, 3447.
6 E. Wang, L. Hou, Z. Wang, S. Hellström, F. Zhang, O. Inganäs and M. R. Andersson, *Adv. Mater.*, 2010, **22**, 5240.
7 J. Li, Z. Liang, Y. Wang, H. Li, J. Tong, X. Bao and Y. Xia, *J. Mater. Chem. C*, 2018, **6**, 11015.
8 J. Li, Y. Wang, Z. Liang, N. Wang, J. Tong, C. Yang, X. Bao and Y. Xia, *ACS Appl. Mater. Interfaces*, 2019, **11**, 7022.
9 Z. He, B. Xiao, F. Liu, H. Wu, Y. Yang, S. Xiao, C. Wang, T. P. Russell and Y. Cao, *Nat. Photonics*, 2015, **9**, 174.
10 H. Zhou, Y. Zhang, C. K. Mai, S. D. Collins, G. C. Bazan, T. Q. Nguyen and A. J. Heeger, *Adv. Mater.*, 2015, **27**, 1767.
11 B. Kan, M. Li, Q. Zhang, F. Liu, X. Wan, Y. Wang, W. Ni, G. Long, X. Yang, H. Feng, Y. Zuo, M. Zhang, F. Huang, Y. Cao, T. P. Russell and Y. Chen, *J. Am. Chem. Soc.*, 2015, **137**, 3886.
12 M. Li, K. Gao, X. Wan, Q. Zhang, B. Kan, R. Xia, F. Liu, X. Yang, H. Feng, W. Ni, Y. Wang, J. Peng, H. Zhang, Z. Liang, H. L. Yip, X. Peng, Y. Cao and Y. Chen, *Nat. Photonics*, 2016, **11**, 85.
13 J. Zhao, Y. Li, G. Yang, K. Jiang, H. Lin, H. Ade, W. Ma and H. Yan, *Nat. Energy*, 2016, **1**, 15027.
14 D. Deng, Y. Zhang, J. Zhang, Z. Wang, L. Zhu, J. Fang, B. Xia, Z. Wang, K. Lu, W. Ma and Z. Wei, *Nat. Commun.*, 2016, **7**, 13740.
15 B. Kan, H. Feng, X. Wan, F. Liu, X. Ke, Y. Wang, Y. Wang, H. Zhang, C. Li, J. Hou and Y. Chen, *J. Am. Chem. Soc.*, 2017, **139**, 4929.
16 Z. M. Zhong, L. J. Bu, P. Zhu, T. Xiao, B. B. Fan, L. Ying, G. H. Lu, G. Yu, F. Huang and Y. Cao, *ACS Appl. Mater. Interfaces*, 2019, **11**, 8350.
17 Y. Q. Liu, P. Cheng, T. F. Li, R. Wang, Y. W. Li, S. Y. Chang, Y. Zhu, H. W. Cheng, K. H. Wei, X. W. Zhan, B. Q. Sun and Y. Yang, *ACS Nano*, 2019, **13**, 1071.
18 M. Deng, X. P. Xu, Y. W. Lee, H. Y. Woo, Z. Z. Bi, W. Ma, Y. Li and Q. Peng, *ACS Appl. Mater. Interfaces*, 2019, **11**, 3308.
19 Q. An, W. Gao, F. Zhang, J. Wang, M. Zhang, K. Wu, X. Ma, Z. Hu, C. Jiao and C. Yang, *J. Mater. Chem. A*, 2018, **6**, 2468.
20 T. Liu, W. Gao, Y. Wang, T. Yang, R. Ma, G. Zhang, C. Zhong, W. Ma, H. Yan and C. Yang, *Adv. Funct. Mater.*, 2019, **29**, 1902155.
21 C. Yan, S. Barlow, Z. Wang, H. Yan, A. K. Y. Jen, S. R. Marder and X. Zhan, *Nat. Rev. Mater.*, 2018, **3**, 18003.
22 J. Zhang, H. S. Tan, X. Guo, A. Facchetti and H. Yan, *Nat. Energy*, 2018, **3**, 720.
23 L. Meng, Y. Zhang, X. Wan, C. Li, X. Zhang, Y. Wang, X. Ke, Z. Xiao, L. Ding, R. Xia, H.-L. Yip, Y. Cao and Y. Chen, *Science*, 2018, **361**, 1094.
24 J. Yuan, Y. Zhang, L. Zhou, G. Zhang, H. L. Yi, T. K. Lau, X. Lu, C. Zhu, H. Peng, P. A. Johnson, M. Leclerc, Y. Cao, J. Ulanski, Y. Li and Y. Zou, *Joule*, 2019, **3**, 1140.
25 X. Xu, K. Feng, Z. Bi, W. Ma, G. Zhang and Q. Peng, *Adv. Mater.*, 2019, **31**, 1901872.
26 T. Liu, Z. Luo, Q. Fan, G. Zhang, L. Zhang, W. Gao, X. Guo, W. Ma, M. Zhang, C. Yang, Y. Li and H. Yan, *Energy Environ. Sci.*, 2018, **11**, 3275.
27 T. Liu, Z. Luo, Y. Chen, T. Yang, Y. Xiao, G. Zhang, R. Ma, X. Lu, C. Zhan, M. Zhang, C. Yang, Y. Li, J. Yao and H. Yan, *Energy Environ. Sci.*, 2019, **2**, 2529.
28 Q. An, X. Ma, J. Gao and F. Zhang, *Sci. Bull.*, 2019, **64**, 504.
29 B. Fan, D. Zhang, M. Li, W. Zhong, Z. Zeng, L. Ying, F. Huang and Y. Cao, *Sci. China: Chem.*, 2019, **62**, 746.
30 S. Zhang, Y. Qin, J. Zhu and J. Hou, *Adv. Mater.*, 2018, **30**, 1800868.
31 Z. Fei, F. D. Eisner, X. Jiao, M. Azzouzi, J. A. Röhr, Y. Han, M. Shahid, A. S. R. Chesman, C. D. Easton, C. R. McNeill, T. D. Anthopoulos, J. Nelson and M. Heeney, *Adv. Mater.*, 2018, **30**, 1705209.
32 T. Liu, W. Gao, G. Zhang, L. Zhang, J. Xin, W. Ma, C. Yang, H. Yan, C. Zhan and J. Yao, *Sol. RRL*, 2019, **3**, 1800376.
33 J. Sun, X. Ma, Z. Zhang, J. Yu, J. Zhou, X. Yin, L. Yang, R. Geng, R. Zhu, F. Zhang and W. Tang, *Adv. Mater.*, 2018, **30**, 1707150.
34 Z. Zhou, S. Xu, J. Song, Y. Jin, Q. Yue, Y. Qian, F. Liu, F. Zhang and X. Zhu, *Nat. Energy*, 2018, **3**, 952.
35 J. Wang, J. Zhang, Y. Xiao, T. Xiao, R. Zhu, C. Yan, Y. Fu, G. Lu, X. Lu, S. R. Marder and X. Zhan, *J. Am. Chem. Soc.*, 2018, **140**, 91407.
36 Z. Luo, T. Liu, Y. Wang, G. Zhang, R. Sun, Z. Chen, C. Zhong, J. Wu, Y. Chen, M. Zhang, Y. Zou, W. Ma, H. Yan, J. Min, Y. Li and C. Yang, *Adv. Energy Mater.*, 2019, **9**, 1900041.
37 Y. Lin, J. Wang, Z.-G. Zhang, H. Bai, Y. Li, D. Zhu and X. Zhan, *Adv. Mater.*, 2015, **27**, 1170.
38 Y. Lin, F. Zhao, Q. He, L. Huo, Y. Wu, T. C. Parker, W. Ma, Y. Sun, C. Wang, D. Zhu, A. J. Heeger, S. R. Marder and X. Zhan, *J. Am. Chem. Soc.*, 2016, **138**, 4955.
39 Y. Lin, Q. He, F. Zhao, L. Huo, J. Mai, X. Lu, C.-J. Su, T. Li, J. Wang, J. Zhu, Y. Sun, C. Wang and X. Zhan, *J. Am. Chem. Soc.*, 2016, **138**, 2973.
40 T. Liu, Z. Luo, Q. Fan, G. Zhang, L. Zhang, W. Gao, X. Guo, W. Ma, M. Zhang, C. Yang, Y. Li and H. Yan, *Energy Environ. Sci.*, 2018, **11**, 3275.
41 C. Duan, G. Zango, M. García Iglesias, F. J. M. Colberts, M. M. Wienk, M. V. Martínez-Díaz, R. A. J. Janssen and T. Torres, *Angew. Chem., Int. Ed.*, 2017, **56**, 148.

42 A. Nowak-Król, K. Shoyama, M. Stolte and F. Würthner, *Chem. Commun.*, 2018, **54**, 13763.
43 H. Sun, X. Song, J. Xie, P. Sun, P. Gu, C. Liu, F. Chen, Q. Zhang, Z. K. Chen and W. Huang, *ACS Appl. Mater. Interfaces*, 2017, **9**, 29924.
44 X. W. Zhan, A. Facchetti, S. Barlow, T. J. Marks, M. A. Ratner, M. R. Wasielewski and S. R. Marder, *Adv. Mater.*, 2011, **23**, 268.
45 J. Wang and X. Zhan, *Trends Chem.*, 2019, DOI: 10.1016/j.trechm.2019.05.002.
46 G. Li, S. H. Wang, T. Liu, P. Hao, Z. Liu, F. Li, L. M. Yang, Y. Zhang, D. Li, S. F. Yang, J. Zhao, J. Li, H. Yan and B. Tang, *J. Mater. Chem. C*, 2018, **6**, 12601.
47 G. Li, Y. Zhang, T. Liu, S. Wang, D. Li, J. Li, F. Li, L. M. Yang, Z. Luo, C. Yang, H. Yan, P. Hao, Q. Shang and B. Tang, *J. Mater. Chem. C*, 2018, **6**, 11111.
48 T. Liu, D. Meng, Y. Cai, X. Sun, Y. Li, L. Huo, F. Liu, Z. Wang, T. P. Russell and Y. Sun, *Adv. Sci.*, 2016, **3**, 1600117.
49 Z. Luo, T. Liu, Z. Chen, Y. Xiao, G. Zhang, L. Huo, C. Zhong, X. Lu, H. Yan, Y. Sun and C. Yang, *Adv. Sci.*, 2019, **6**, 1802065.
50 Y. Duan, X. Xu, H. Yan, W. Wu, Z. Li and Q. Peng, *Adv. Mater.*, 2017, **29**, 1605115.
51 S. Li, W. Liu, C. Z. Li, T. K. Lau, X. Lu, M. Shi and H. A. Chen, *J. Mater. Chem. A*, 2016, **4**, 14983.
52 Q. Wu, D. Zhao, A. M. Schneider, W. Chen and L. Yu, *J. Am. Chem. Soc.*, 2016, **138**, 7248.
53 D. Sun, D. Meng, Y. Cai, B. Fan, Y. Li, W. Jiang, L. Huo, Y. Sun and Z. Wang, *J. Am. Chem. Soc.*, 2015, **137**, 11156.
54 D. Meng, D. Sun, C. Zhong, T. Liu, B. Fan, L. Huo, Y. Li, W. Jiang, H. Choi, T. Kim, J. Y. Kim, Y. Sun, Z. Wang and A. J. Heeger, *J. Am. Chem. Soc.*, 2016, **138**, 375.
55 J. Zhang, Y. Li, J. Huang, H. Hu, G. Zhang, T. Ma, P. C. Y. Chow, H. Ade, D. Pan and H. Yan, *J. Am. Chem. Soc.*, 2017, **139**, 16092.
56 R. Wang, G. Li, A. Zhang, W. Wang, G. Cui, J. Zhao, Z. Shi and B. Tang, *Chem. Commun.*, 2017, **53**, 6918.
57 M. J. Frisch and G. W. Trucks, *et al.*, *Gaussian 09*, Gaussian, Inc., Wallingford, CT, 2009, see ESI† for full citation.
58 T. Liu, L. Huo, S. Chandrabose, K. Chen, G. Han, F. Qi, X. Meng, D. Xie, W. Ma, Y. Yi, J. M. Hodgkiss, F. Liu, J. Wang, C. Yang and Y. Sun, *Adv. Mater.*, 2018, **30**, 1707353.

